Frontiers of Information Technology & Electronic Engineering
www.zju.edu.cn/jzus; engineering.cae.cn; www.springerlink.com
ISSN 2095-9184 (print); ISSN 2095-9230 (online)
E-mail: jzus@zju.edu.cn

Initial position estimation strategy for a surface permanent magnet synchronous motor used in hybrid electric vehicles*

Bing TIAN, Qun-tao AN, Li SUN†‡, Dong-yang SUN, Jian-dong DUAN

(*Department of Electrical Engineering, Harbin Institute of Technology, Harbin 150001, China*)

†E-mail: motor611@sina.com

Received Sept. 10, 2015; Revision accepted Feb. 25, 2016; Crosschecked July 12, 2016

Abstract: A novel nonlinear model for surface permanent magnet synchronous motors (SPMSMs) is adopted to estimate the initial rotor position for hybrid electric vehicles (HEVs). Usually, the accuracy of initial rotor position estimation for SPMSMs relies on magnetic saturation. To verify the saturation effect, the transient finite element analysis (FEA) model is presented first. Hybrid injection of a static voltage vector (SVV) superimposed with a high-frequency rotating voltage is proposed. The magnetic polarity is roughly identified with the aid of the saturation evaluation function, based on which an estimation of the position is performed. During this procedure, a special demodulation is suggested to extract signals of iron core saturation and rotor position. A Simulink/MATLAB platform for SPMSMs at standstill is constituted, and the effectiveness of the proposed strategy is verified. The proposed method is also validated by experimental results of an SPMSM drive.

Key words: Surface permanent magnet synchronous motor (SPMSM), Initial position estimation, Nonlinear model, Hybrid injection, Position observer

http://dx.doi.org/10.1631/FITEE.1500298 **CLC number:** TM301.2

1 Introduction

Hybrid electric vehicles (HEVs) are one of the main trends in current vehicle development. Adding supplemental energy storage and energy conversion devices to conventionally powered passenger cars allows vehicle manufacturers to significantly increase energy usage efficiency of the overall vehicle. In these vehicles, essential requirements for the electric drive are low weight, small size, high efficiency, and low cost. When selecting a motor for the vehicle drive, a surface permanent magnet synchronous motor (SPMSM) is an obvious option for high efficiency and simple structure (Sigmund *et al*., 2014). Usually, a mechanical position sensor mounted on the shaft is incorporated in the drive for sinusoidal AC brushless drives, to guarantee field-oriented control and low torque ripples. Clearly, this would increase the cost and complexity of the electric drive. To overcome these drawbacks, sensorless control methods have attracted great attention during the past few years (Bolognani *et al*., 2011). Among various sensorless control methods, position estimation at low speeds is still a challenge. Normally, sensorless control methods at low speeds including standstill can be categorized into three types: high-frequency (HF) rotating voltage injection, HF pulsating voltage injection, and square wave injection (Yang, 2015). Because the inherent saliency ratio of SPMSMs (ratio between *q*- and *d*-axis self-inductances, i.e., L_{qq}/L_{dd}) is quite small compared with that of an interior permanent magnet synchronous motor (IPMSM), it is arduous to estimate rotor position for SPMSMs with

‡ Corresponding author

* Project supported by the National Natural Science Foundation of China (Nos. 51207029 and 51507039), the Fundamental Research Funds for the Central Universities, China (No. HIT.NSRIF.2017013), and the China Postdoctoral Science Foundation (No. 2016M591529)

ORCID: Bing TIAN, http://orcid.org/0000-0003-4977-2362

conventional approaches. A compromise, but a viable option, for sensorless control, is to adopt a low-resolution Hall effect position sensor, which provides a typical resolution of 60° (electrical). Extraction for a high-resolution position from binary Hall effect sensors was detailed in Harke *et al*. (2008). However, such an algorithm cannot be used when the motor starts due to a large position estimation error (up to 60°). An accurate initial position estimation is needed to help start HEVs under a heavy load condition.

In most studies, rotor position estimation for SPMSMs was completed with the aid of magnetic saturation effect (Seilmeier and Piepenbreier, 2011); i.e., the iron core is easier to saturate in the magnetic direction, and hence L_{dd} and L_{qq} could be made different. In Nakashima *et al*. (2000), position estimation was based on the mechanism that phase current response increases when the corresponding phase gets close to the magnetic polarity. Then a sequence of voltage vectors was applied to the stator winding, and rotor position was obtained via comparison of current responses. Wang *et al.* (2012) used finite element analysis (FEA) to model a brushless DC motor. By injecting voltage from phase A and measuring the current responses in phases B and C, rotor position can be identified through comparison of response amplitudes. However, the estimation precision is up to 60^{o} (electrical), so the applications of this method are restricted. In Fu *et al.* (2009), the FEA method was also used to estimate the rotor position at standstill for a two-phase permanent magnet (PM) motor. The basic approach is to inject an HF voltage from phase A and then to measure the induced electromotive force (EMF) of phase B. A variable incorporating self- and mutual-inductance was introduced to improve estimation accuracy. However, a large number of preparatory measurements still need to be completed. In Li *et al*. (2007), the self-inductances L_{dd} and L_{qq} were measured based on the HF signal-injection method, and then they were used to compensate for the position estimation error for a brushless AC motor at low speeds. Since all necessary parameters are acquired by either the FEA method or measurements in advance, the application of this method is also restricted. In Yan *et al*. (2008), voltage pulses were applied to detect the saturation saliency, and magnetic polarity was determined by comparison of peak current. However, in the test drive, the current peak value was sampled at a fixed time, and it is difficult to obtain the amplitude of the triangle current response without a demodulation algorithm.

Magnetic saturation in the iron core leads to flux linkages between the *d*- and *q*-axis, and hence increases the difficulties in modeling a PM motor. Gao *et al*. (2005) proposed a nonlinear synchronous machine model in a phase frame. However, the model is so complicated that it is difficult to apply in sensorless control applications. In Wang *et al*. (2010), self- and mutual-inductances, considering structural and saturation saliencies, were investigated based on Fourier series. Then a peak current comparison method was performed to estimate the rotor position. A comprehensive mathematical model considering the magnetic saturation effect was further suggested for PM machines, and the accuracy of the proposed nonlinear model was verified by experiments.

In this paper, an initial rotor position estimation exploiting a nonlinear SPMSM model, as described in Wang *et al*. (2010), is proposed to improve position estimation accuracy. Since L_{dd} and L_{qq} have no significant difference, it is difficult to estimate the rotor position at low speeds. This means that there presents no spatial saliency for an SPMSM and that the HF current cannot be modulated by rotor position. In this case, saturating the iron core before estimating rotor position provides a solution for SPMSMs. The proposed strategy has the following innovative features: (1) Iron core saturation is depicted under different excitation currents; (2) The hybrid injection method is introduced, which consists of a static voltage vector (SVV) and an HF rotating voltage vector, and thus the machine saturation level can be altered by the SVV; (3) Magnetic polarity is roughly identified by comparing the saturation evaluation function, and then the most saturated machine can be obtained by fixing the SVV at this estimated magnetic polarity; (4) Saturation evaluation function and rotor position information is extracted with an easy-to-implement demodulation algorithm; (5) A position observer is adopted to improve the accuracy of the estimated position. The entire strategy is tested by simulation and experiment, and the results show that the proposed method has a high precision in estimating the initial rotor position for SPMSMs.

2 Principle and verification

2.1 Principle of magnetic saturation effect

The magnetic saturation effect exists in PM machines. When taking into account this phenomenon, the nonlinear model for PM motors in a *d*-*q* frame can be written as (Liang *et al*., 2010)

$$\begin{bmatrix} u_d \\ u_q \end{bmatrix} = R\begin{bmatrix} i_d \\ i_q \end{bmatrix} + \begin{bmatrix} L_{dd} & L_{dq} \\ L_{qd} & L_{qq} \end{bmatrix} p\begin{bmatrix} i_d \\ i_q \end{bmatrix} + \omega_e \begin{bmatrix} -\psi_q \\ \psi_d \end{bmatrix}, \quad (1)$$

$$\begin{bmatrix} L_{dd} & L_{dq} \\ L_{qd} & L_{qq} \end{bmatrix} = \begin{bmatrix} \dfrac{\partial \psi_d}{\partial i_d} & \dfrac{\partial \psi_d}{\partial i_q} \\ \dfrac{\partial \psi_q}{\partial i_d} & \dfrac{\partial \psi_q}{\partial i_q} \end{bmatrix}, \quad (2)$$

where R is the stator resistance, p the differential operator, ω_e the electrical angular velocity of the rotor, u_d and u_q the *d*- and *q*-axis stator voltages, respectively, i_d and i_q the *d*- and *q*-axis stator currents, respectively, L_{dd} and L_{qq} the *d*- and *q*-axis self-inductances, respectively, ψ_d and ψ_q the *d*- and *q*-axis flux linkages, respectively, and L_{dq} and L_{qd} the *d*- and *q*-axis mutual-inductances, respectively.

For SPMSMs, the saliency ratio (L_{qq}/L_{dd}) is vanishingly small, which is essential for rotor position estimation at low speeds. However, the saliency ratio can be altered by a stator excitation current, and thus provides a solution for detecting rotor position. Iron core saturation takes place in the direction of the total equivalent excitation current (Fig. 1). The equivalent excitation current can be illustrated by (El-Serafi and Wu, 1993)

$$\boldsymbol{i}_t = \boldsymbol{i}_s + \boldsymbol{i}_f, \quad (3)$$

where $\boldsymbol{i}_f$ represents the equivalent excitation current vector of the PM, $\boldsymbol{i}_s$ the stator current vector, and $\boldsymbol{i}_t$ the resultant excitation current vector.

By projecting $\boldsymbol{i}_t$ onto the *d*- and *q*-axis, respectively, as shown in Fig. 1, one can derive

$$i_{dt} = \| \boldsymbol{i}_t \| \cos\delta = i_d + \| \boldsymbol{i}_f \|, \quad (4)$$

$$i_{qt} = i_q = \| \boldsymbol{i}_t \| \sin\delta, \quad (5)$$

$$\psi_d = \psi(\| \boldsymbol{i}_t \|)\cos\delta, \quad (6)$$

$$\psi_q = \psi(\| \boldsymbol{i}_t \|)\sin\delta, \quad (7)$$

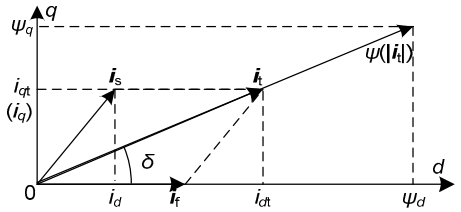

Fig. 1 Vector decomposition for flux linkage and excitation current

where i_{dt} and i_{qt} are the *d*-*q* frame equivalent excitation currents, respectively, δ the direction of $\boldsymbol{i}_t$ in the *d*-*q* frame, $\psi()$ the flux linkage function of the iron core, and $\|\cdot\|$ the vector magnitude.

Hence, self-inductances of the *d*-*q* frame can be derived as

$$L_{dd} = \frac{\partial \psi_d}{\partial i_d} = \frac{\mathrm{d}\psi(i_{dt})}{\mathrm{d}i_{dt}}, \quad (8)$$

$$L_{qq} = \frac{\partial \psi_q}{\partial i_q} = \frac{\mathrm{d}\psi(i_{qt})}{\mathrm{d}i_{qt}}. \quad (9)$$

L_{dd} and L_{qq} are tangent-slope inductances, as shown in Fig. 2. The iron core will become saturated when δ is located between 0 and 90° (electrical). In such conditions, an artificial magnetic saliency for SPMSMs is acquired, i.e., $L_{qq}/L_{dd}>1$.

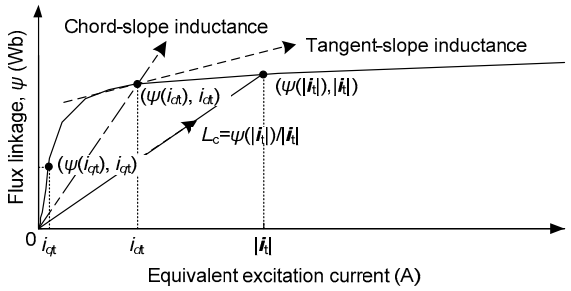

Fig. 2 Magnetic property for the iron core

The magnetic saturation also introduces mutual-flux linkages, which can be expressed as

$$\psi_{dq} = \psi_d - \psi(i_{dt}), \quad (10)$$

$$\psi_{qd} = \psi_q - \psi(i_{qt}), \quad (11)$$

where ψ_{dq} and ψ_{qd} are mutual-flux linkages. The corresponding mutual-inductances are derived as

$$L_{dq}=\frac{\partial\psi_d}{\partial i_q}=\frac{\partial\psi_{dq}}{\partial i_q}, \tag{12}$$

$$L_{qd}=\frac{\partial\psi_q}{\partial i_d}=\frac{\partial\psi_{qd}}{\partial i_d}. \tag{13}$$

Thus, the inductance matrix in Eq. (1) can be obtained as (Wang *et al.*, 2010)

$$\begin{bmatrix}L_{dd} & L_{dq}\\ L_{qd} & L_{qq}\end{bmatrix}=\begin{bmatrix}L_c(1-k_{sat}\cos^2\delta) & -0.5L_c\sin(2\delta)\\ -0.5L_c\sin(2\delta) & L_c(1-k_{sat}\sin^2\delta)\end{bmatrix}, \tag{14}$$

$$k_{sat}=\frac{L_c-L_t}{L_c},\quad k_{sat}\in(0,1), \tag{15}$$

$$L_c=\frac{\psi(\|\boldsymbol{i}_t\|)}{\|\boldsymbol{i}_t\|},\ L_t=\frac{\mathrm{d}\psi(\|\boldsymbol{i}_t\|)}{\mathrm{d}\|\boldsymbol{i}_t\|}, \tag{16}$$

where L_c is the chord-slope inductance, L_t the tangent slope inductance (Fig. 2), and k_{sat} a saturation variable. In fact, values of k_{sat} and $1/L_c$ increase when the motor becomes more saturated. As can be seen from Eq. (14), δ will introduce an error into rotor position estimation, and it is crucial to reduce this adverse impact.

2.2 Verification for magnetic saturation effect

To illustrate the nonlinear model, a prototype SPMSM is designed using Ansoft/Maxwell software. The inductance matrix is calculated by 2D FEA. During the simulation, the SPMSM is excited by $\boldsymbol{i}_s$, and hence the motor saturation level can be altered. Note that $\boldsymbol{i}_s$ represents the injected low-frequency excitation current, which is used to alter motor saturation, and it is different from HF injection signals.

The simulation is performed with δ=0, and is rotating synchronously with the rotor. The characteristics for L_{dd}- and L_{qq}-position are computed with different $\boldsymbol{i}_s$ (Fig. 3). The simulation parameters are listed in Table 1.

As can be seen from Fig. 3, L_{dd} and L_{qq} decrease when the SPMSM becomes more saturated, and L_{dd} changes much more significantly than L_{qq} (L_{dd} and L_{qq} are equal at $\|\boldsymbol{i}_s\|$=0, but differ remarkably at $\|\boldsymbol{i}_s\|$=10 A). However, the cause of the slot effect is fluctuation of L_{dd} and L_{qq} as the rotor rotates. Fortunately, this adverse factor can be ignored since the rotor does not rotate.

The results imply that by injecting $\boldsymbol{i}_s$ into the magnetic direction, L_{dd} and L_{qq} can be altered. Providing that this saturation is large enough, it is feasible to estimate rotor position for SPMSMs. In this study, only the initial position estimation for SPMSMs is investigated, and the primary concern should be how to saturate the machine.

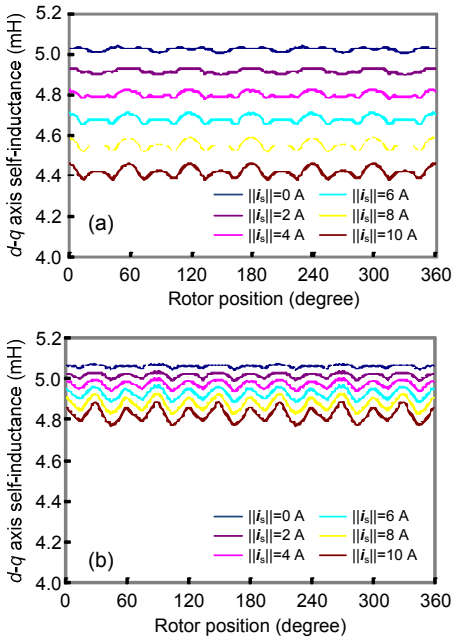

Fig. 3 Inductance-position characteristics: (a) L_{qq}-position; (b) L_{dd}-position (References to color refer to the online version of this figure)

Table 1 Ansoft/Maxwell simulation parameters

Description	Value
Amplitude of $\boldsymbol{i}_s$	0, 2, 4, 6, 8, 10 A
Angular velocity of $\boldsymbol{i}_s$	2π×50 rad/s
Pole pairs	4
Angular velocity of rotor	2π×50/4 rad/s
Initial rotor position	0°
Stator slot number	28

3 Proposed initial position detection strategy

3.1 Definition of saturation evaluation function

The nonlinear model for SPMSMs in the *d-q* frame lacks rotor position information, and therefore it must be transformed to the *α-β* frame. The HF model for SPMSMs at standstill is established as in Eqs. (17) and (18). Generally, the stator resistance is

much smaller than the HF impedance and can be neglected.

$$\begin{bmatrix} u_{\alpha\mathrm{h}} \\ u_{\beta\mathrm{h}} \end{bmatrix} = R\begin{bmatrix} i_{\alpha\mathrm{h}} \\ i_{\beta\mathrm{h}} \end{bmatrix} + \begin{bmatrix} L_{\alpha\alpha} & L_{\alpha\beta} \\ L_{\beta\alpha} & L_{\beta\beta} \end{bmatrix} p\begin{bmatrix} i_{\alpha\mathrm{h}} \\ i_{\beta\mathrm{h}} \end{bmatrix}, R \approx 0, \quad (17)$$

$$\begin{bmatrix} L_{\alpha\alpha} & L_{\alpha\beta} \\ L_{\beta\alpha} & L_{\beta\beta} \end{bmatrix} = \begin{bmatrix} L_{\mathrm{c}}(1-k_{\mathrm{sat}}\cos^2(\delta+\theta_{\mathrm{d0}})) & -0.5L_{\mathrm{c}}\sin(2(\delta+\theta_{\mathrm{d0}})) \\ -0.5L_{\mathrm{c}}\sin(2(\delta+\theta_{\mathrm{d0}})) & L_{\mathrm{c}}(1-k_{\mathrm{sat}}\sin^2(\delta+\theta_{\mathrm{d0}})) \end{bmatrix}, \quad (18)$$

where $u_{\alpha\mathrm{h}}$ and $u_{\beta\mathrm{h}}$ are the α-β axis HF stator voltages, respectively, $i_{\alpha\mathrm{h}}$ and $i_{\beta\mathrm{h}}$ the α-β axis HF current responses, respectively, $L_{\alpha\alpha}$ and $L_{\beta\beta}$ the α-β axis self-inductances, respectively, and $L_{\alpha\beta}$ and $L_{\beta\alpha}$ the α-β axis mutual-inductances, respectively.

The HF rotating voltage can be injected with the aid of a voltage-source inverter, and the HF voltage vector is expressed by

$$[u_{\alpha\mathrm{h}} \quad u_{\beta\mathrm{h}}]^{\mathrm{T}} = v_{\mathrm{im}}[\cos(\omega_{\mathrm{ih}}t) \quad \sin(\omega_{\mathrm{ih}}t)], \quad (19)$$

where v_{im} indicates the magnitude of the injected HF voltage vector, and ω_{ih} is the angular velocity of this HF voltage vector.

By solving Eqs. (18) and (19), one can obtain

$$\begin{aligned} \begin{bmatrix} i_{\alpha\mathrm{h}} \\ i_{\beta\mathrm{h}} \end{bmatrix} &= I_{\mathrm{P}}\begin{bmatrix} \cos\left(\omega_{\mathrm{ih}}t-\frac{\pi}{2}\right) \\ \sin\left(\omega_{\mathrm{ih}}t-\frac{\pi}{2}\right) \end{bmatrix} \\ &\quad + I_{\mathrm{N}}\begin{bmatrix} \cos\left(2\delta+2\theta_{\mathrm{d0}}-\omega_{\mathrm{ih}}t+\frac{\pi}{2}\right) \\ \sin\left(2\delta+2\theta_{\mathrm{d0}}-\omega_{\mathrm{ih}}t+\frac{\pi}{2}\right) \end{bmatrix}, \end{aligned} \quad (20)$$

$$I_{\mathrm{P}} = \frac{v_{\mathrm{im}}}{\omega_{\mathrm{ih}}}\frac{2-k_{\mathrm{sat}}}{2L_{\mathrm{c}}(1-k_{\mathrm{sat}})}, \quad k_{\mathrm{sat}} \in (0,1), \quad (21)$$

$$I_{\mathrm{N}} = \frac{v_{\mathrm{im}}}{\omega_{\mathrm{ih}}}\frac{k_{\mathrm{sat}}}{2L_{\mathrm{c}}(1-k_{\mathrm{sat}})}, \quad k_{\mathrm{sat}} \in (0,1). \quad (22)$$

From a phasor point of view, Eq. (20) can be rewritten as

$$\boldsymbol{i}_{\alpha\beta}^{\mathrm{h}} = \underbrace{I_{\mathrm{P}}\exp\left(\mathrm{j}\left(\omega_{\mathrm{ih}}t-\frac{\pi}{2}\right)\right)}_{\text{Positive-sequence component}} + \underbrace{I_{\mathrm{N}}\exp\left(\mathrm{j}\left(2\delta+2\theta_{\mathrm{d0}}-\omega_{\mathrm{ih}}t+\frac{\pi}{2}\right)\right)}_{\text{Negative-sequence component}}. \quad (23)$$

The second term of Eq. (23) represents a negative-sequence component, and it contains rotor position information when $I_{\mathrm{N}}\neq 0$. This means that the tested machine must be saturated. Hereafter, the saturation evaluation function is defined by

$$\begin{aligned} f_{\mathrm{sat}} &= I_{\mathrm{P}}^2 + I_{\mathrm{N}}^2 \\ &= \left(\frac{v_{\mathrm{im}}}{\sqrt{2}L_{\mathrm{c}}\omega_{\mathrm{ih}}}\right)^2\left(1+\frac{1}{(1-k_{\mathrm{sat}})^2}\right), \ k_{\mathrm{sat}} \in (0,1). \end{aligned} \quad (24)$$

f_{sat} shows a positive correlation with k_{sat} and $1/L_{\mathrm{c}}$, and increases when the iron core becomes saturated. f_{sat} can be easily extracted by signal processing techniques, and is later used for the identification of magnetic polarity.

3.2 Saturation-based magnetic polarity identification

The signal injected into a real motor consists of two parts: the static voltage vector (SVV) in the estimated d-q frame, and the superimposed HF rotating voltage in the α-β frame (Fig. 4). The SVV alters the motor saturation level. The HF current, which is due to HF voltage injection, is modulated by magnetic saliency. Note that the magnitude of HF current should be much smaller than that of $\boldsymbol{i}_{\mathrm{s}}$. The injected signals can be expressed by the following matrix:

$$\begin{bmatrix} v_\alpha^* \\ v_\beta^* \end{bmatrix} = \boldsymbol{T}_{dq\text{-}\alpha\beta}(\theta_{\hat{d}})\begin{bmatrix} v_{\hat{d}} \\ v_{\hat{q}} \end{bmatrix} + v_{\mathrm{im}}\begin{bmatrix} \cos(\omega_{\mathrm{ih}}t) \\ \sin(\omega_{\mathrm{ih}}t) \end{bmatrix}, \ v_{\hat{q}} \equiv 0, \quad (25)$$

where '^' indicates components of the estimated d-q frame, and '*' stands for control inputs.

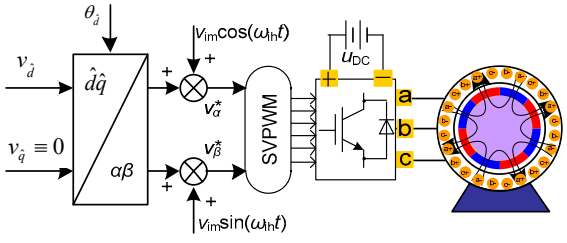

Fig. 4 Block diagram for hybrid injection

According to Eq. (1), the induced $\boldsymbol{i}_s$ can be expressed by

$$\boldsymbol{i}_s=\begin{bmatrix} i_{\hat{d}} \\ i_{\hat{q}} \end{bmatrix}=\frac{1}{R}\begin{bmatrix} v_{\hat{d}} \\ v_{\hat{q}} \end{bmatrix}=\frac{1}{R}\begin{bmatrix} v_{\hat{d}} \\ 0 \end{bmatrix}, \tag{26}$$

$$|\boldsymbol{i}_s|=\sqrt{i_{\hat{d}}^2+i_{\hat{q}}^2}=i_{\hat{d}}. \tag{27}$$

Note that the inductance matrix (Eq. (14)) affects only the transient process and not the steady state values of the stator currents.

The amplitude of $\boldsymbol{i}_t$, shown in Fig. 5, can be derived as

$$\begin{aligned}|\boldsymbol{i}_t|&=\sqrt{(\|\boldsymbol{i}_s\|\cos\zeta+\|\boldsymbol{i}_f\|)^2+(\|\boldsymbol{i}_s\|\sin\zeta)^2}\\&=\frac{\sqrt{R^2\|\boldsymbol{i}_f\|^2+2v_{\hat{d}}\|\boldsymbol{i}_f\|R\cos\zeta+v_{\hat{d}}^2}}{R},\end{aligned} \tag{28}$$

$$\zeta=\theta_{\hat{d}}-\theta_{d0},\ \theta_{\hat{d}}\in(0,2\pi], \tag{29}$$

where ζ is the angle error between the estimated and actual d-axis, and θ_{it} is the direction of $\boldsymbol{i}_t$ (Fig. 5).

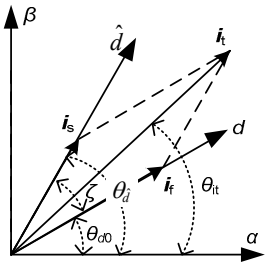

Fig. 5 Vector diagram for excitation current inside the motor, ignoring the weak HF current

Eq. (28) shows that the maximum magnitude of $\boldsymbol{i}_t$ is achieved when the estimated d-axis coincides with the actual one, i.e., ζ=0. In fact, the larger the $\|\boldsymbol{i}_t\|$, the smaller the f_{sat}. Therefore, by comparing f_{sat} when $\boldsymbol{i}_s$ traverses the α-β plane, the magnetic polarity can be roughly identified. The procedures are depicted in an example (Fig. 6).

In the first step, an SVV is applied in the motor, which commutates from 0° to 360°; the commutation interval for each step is 45°. Therefore, the angle plane can be divided into eight sectors (Fig. 6). The initial rotor position is assumed to be 340°, and then the optimal and suboptimal angles, e.g., 315° and 360° (corresponding to the maximum and secondary maximum, respectively) of f_{sat} can be acquired. This means that the rotor position is located in sector VIII. In this case, the intermediate angle 337.5° is taken as the magnetic polarity. Also, note that SVV should be sustained for a period each time until a steady state of $\boldsymbol{i}_s$ is achieved.

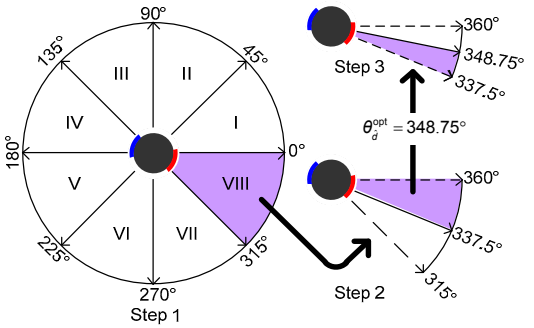

Fig. 6 Saturation-based magnetic polarity identification

In the second step, an SVV at the intermediate angle, i.e., 337.5°, is applied to the windings, and then comparisons are performed with its adjacent vectors. Thus, another two new optimal and suboptimal angles are acquired. Similarly, intermediate angle $\theta_{\hat{d}}^{opt}$ (348.75°) is supposed to be approximate to the actual magnetic polarity. Thus, after several iterations the newest angle obtained by this means could infinitely approach the actual position θ_{d0}.

Since the estimation accuracy also depends on the sensitivity of f_{sat} to the angle step, only the first stage of comparisons is considered with estimation accuracy of up to ±25°. It is high enough to identify the magnetic polarity for SPMSMs. Then the most saturated machine can be acquired by locating the SVV at $\theta_{\hat{d}}^{opt}$.

3.3 Proposed demodulation algorithm

Iron core saturation and rotor position information is included in the HF current response. Hence, a band-pass filter, of which the center frequency is ω_{ih}, is introduced to extract the position information:

$$\boldsymbol{i}_{\alpha\beta}^{h}=\mathrm{BPF}(\boldsymbol{i}_{\alpha\beta}^{h+DC})=i_{\alpha h}+\mathrm{j}i_{\beta h}, \tag{30}$$

where BPF(·) indicates the band-pass filter, $\boldsymbol{i}_{\alpha\beta}^{h+DC}$ is the total current response, and $\boldsymbol{i}_{\alpha\beta}^{h}$ is the HF current response, as shown in Eq. (20). Then, function f_{sat} can be derived by

$$f_{\text{sat}}^{\text{h+DC}} = i_{\alpha\text{h}} \cdot i_{\alpha\text{h}} + i_{\beta\text{h}} \cdot i_{\beta\text{h}} = \underbrace{I_{\text{P}}^2 + I_{\text{N}}^2}_{\text{DC component } f_{\text{sat}}} \underbrace{-2I_{\text{P}}I_{\text{N}}\cos(2(\omega_{\text{ih}}t - \delta - \theta_{d0}))}_{\text{2nd-harmonic frequency component}}, \quad (31)$$

$$f_{\text{sat}} = \text{LPF}(f_{\text{sat}}^{\text{h+DC}}), \quad k_{\text{sat}} \in (0,1), \quad (32)$$

where $f_{\text{sat}}^{\text{h+DC}}$ is a temporary variable, and LPF represents a low-pass filter. Clearly, f_{sat} is easy to acquire via a simple LPF, whereas rotor position variables can be extracted by

$$\boldsymbol{i}_{\text{N}}^{\text{h+DC}} = \boldsymbol{i}_{\alpha\beta}^{\text{h}}\exp(\text{j}\omega_{\text{ih}}t) = \underbrace{I_{\text{P}}\exp\left(\text{j}\left(2\omega_{\text{ih}}t - \frac{\pi}{2}\right)\right)}_{\text{2nd-harmonic frequency component}} + \underbrace{I_{\text{N}}\exp\left(\text{j}\left(2\delta + 2\theta_{d0} + \frac{\pi}{2}\right)\right)}_{\text{DC ingredient}}, \quad (33)$$

$$\boldsymbol{I}_{\text{N}}^{\text{DC}} = \text{LPF}(\boldsymbol{i}_{\text{N}}^{\text{h+DC}}) = I_{\text{N}}\exp\left(\text{j}\left(2\delta + 2\theta_{d0} + \frac{\pi}{2}\right)\right), \quad (34)$$

where $\boldsymbol{i}_{\text{N}}^{\text{h+DC}}$ is a temporary variable, and $\boldsymbol{I}_{\text{N}}^{\text{DC}}$ is the DC component containing rotor position information. The following discusses how to reduce the position estimation error by using $\boldsymbol{I}_{\text{N}}^{\text{DC}}$.

3.4 Position observer

To improve the accuracy of the position estimation, a position observer is suggested after identifying the magnetic polarity.

Fig. 7 shows the principle of a closed-loop position observer, in which the term $2\delta+2\theta_{d0}+\pi/2$ in Eq. (34) is substituted by θ_{ob} for simplification. By demodulating the vector $I_{\text{N}}\exp(\text{j}\theta_{\text{ob}})$ with feedback signals, the phase error $I_{\text{N}}\Delta\theta_{\text{ob}}$ can be derived, as depicted in Eq. (35), and converges to zero with a proportional-integral (PI) controller. Accordingly, phase error signal can be presented by

$$I_{\text{N}}\Delta\theta_{\text{ob}} \approx I_{\text{N}}\sin\Delta\theta_{\text{ob}} = I_{\text{N}}\sin(\theta_{\text{ob}} - \hat{\theta}_{\text{ob}}) = I_{\text{N}}\sin\theta_{\text{ob}}\cos\hat{\theta}_{\text{ob}} - I_{\text{N}}\cos\theta_{\text{ob}}\sin\hat{\theta}_{\text{ob}}, \quad (35)$$

where $\hat{\theta}_{\text{ob}}$ is the position observer output. Note that Eq. (35) is valid only when $\Delta\theta_{\text{ob}}$ is small enough. Since the observed angle is the DC component because of motor standstill, a PI controller is sufficient for this type of position estimation. After some tuning time with PI, $\hat{\theta}_{\text{ob}}$ is approximate to the true value, and by setting $2\delta+2\theta_{d0}+\pi/2$ to $\hat{\theta}_{\text{ob}}$, one can obtain

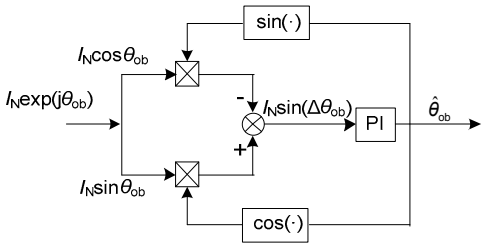

Fig. 7 Block diagram for a position observer

$$\theta_{\text{it}}' = \theta_{d0} + \delta = \frac{\hat{\theta}_{\text{ob}} - \pi/2}{2}, \quad (36)$$

where θ_{it}' indicates the estimated direction of $\boldsymbol{i}_{\text{t}}$. The relationship between θ_{it}' and θ_{d0} is indicated in Fig. 1. Note that at the present time θ_{it}' may represent the bi-direction of $\boldsymbol{i}_{\text{t}}$, and the actual direction of $\boldsymbol{i}_{\text{t}}$ can be determined with the aid of $\theta_{\hat{d}}^{\text{opt}}$:

$$\hat{\theta}_{\text{it}} = \begin{cases} \theta_{\text{it}}' + \pi, & |\theta_{\text{it}}' - \theta_{\text{d}}^{\text{opt}}| \notin \left(\pi - \frac{5}{36}\pi,\ \pi + \frac{5}{36}\pi\right), \\ \theta_{\text{it}}', & \text{otherwise}, \end{cases} \quad (37)$$

where the error angle ±25° is due to the estimated error in magnetic polarity. Thus, the estimated rotor position is

$$\hat{\theta}_{d0} = \hat{\theta}_{\text{it}} - \delta, \quad \delta \to 0, \quad (38)$$

where $\hat{\theta}_{d0}$ is the estimated rotor position. Although δ affects the estimation accuracy, it is infinitesimally small and can be a neglected cause of SVV aligning to the *d*-axis, as shown in Fig. 5.

4 Simulation results and discussion

The proposed initial rotor position estimation is investigated on the Simulink/MATLAB platform, and the nonlinear model of SPMSMs at standstill is built by the MATLAB S-function (Fig. 8). In the

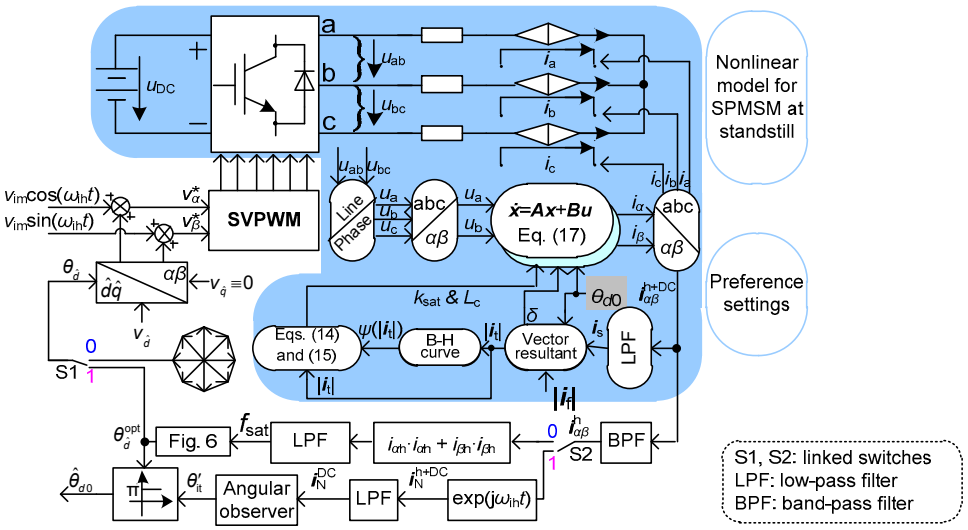

Fig. 8 Overall control strategy for the simulation platform

simulation platform, the insulated gate bipolar translator (IGBT) module is assumed to be ideal, and its switching frequency is 10 kHz. The B-H curve is established using a classical fitting method according to nonlinear magnetization data of the iron core. S1 and S2 switching to '0' means that only magnetic polarity identification is carried out, and '1' indicates that the position observer is performed. An LPF with a cut-off frequency of 200 Hz is selected as the inertial filter, whereas the center frequency of the BPF is set at 500 Hz. Other parameters for the simulation platform are listed in Table 2.

Table 2 MATLAB simulation parameters

Parameter	Value
Stator resistance, R	1.28 Ω
PM flux linkage, ψ_f	0.275 Wb
Pole pairs, P	4
Amplitude of the SVV	9 V
Amplitude of HF voltage, v_{im}	6 V
Initial rotor position, θ_{d0}	184.5°

Fig. 9 shows the total current response in the α-β frame including $\boldsymbol{i}_s$ and Fig. 10 shows the HF current $\boldsymbol{i}^h_{\alpha\beta}$ (500 Hz), which is attributed to the hybrid injection of SVV and HF voltage. In the simulation, SVV commutates from 0° to 360°, and the commutation interval is 45° and achieves a steady state within 0.07 s. As can be seen from Fig. 10, $\boldsymbol{i}_s$ is in phase with SVV, and would affect the saturation evaluation function f_{sat}. As can be seen from Fig. 11, f_{sat} varies with estimated position, and magnetic polarity can be roughly identified. In Fig. 11, two optimal and suboptimal angles, i.e., 180° and 225°, corresponding to the maximum and secondary maximum of f_{sat}, respectively, are acquired; the intermediate value $\theta^{opt}_{\hat{d}}$ (202.5°) is considered to be the magnetic polarity in this procedure.

After roughly identifying the magnetic polarity, the direction of SVV is initially set at $\theta^{opt}_{\hat{d}}$ (202.5°).

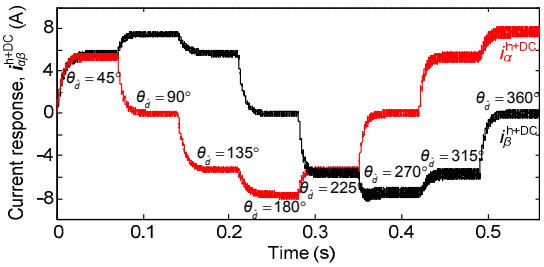

Fig. 9 Total current response in the α-β frame

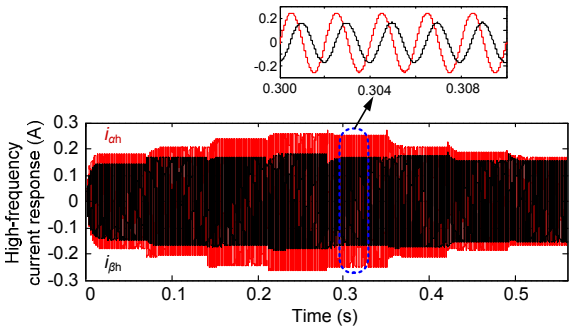

Fig. 10 Simulation results for extracting 500 Hz currents

determine the estimated position. Fig. 12 illustrates the trajectory of the HF current response when the SVV is located at 202.5°. As shown, the current vector rotates elliptically in the α-β plane, and there emerges a negative-sequence component which includes rotor position information. The estimation results are shown in Fig. 13, and the estimation error is less than −3.6°.

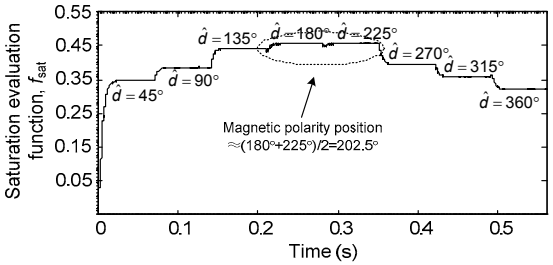

Fig. 11 Simulation process for identification of magnetic polarity

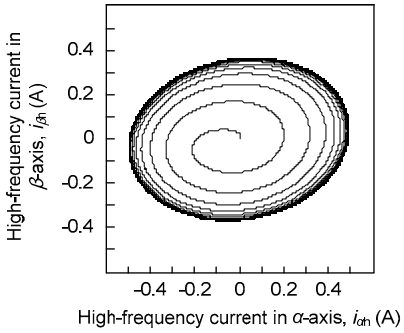

Fig. 12 Trajectory of the HF current vector

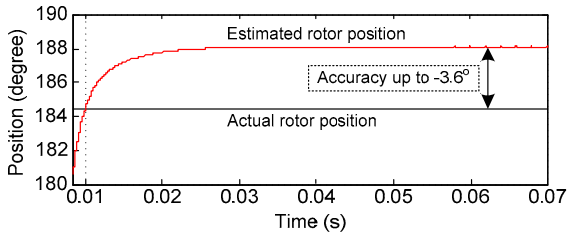

Fig. 13 Simulation performance of the position observer

5 Measurement results

The SPMSM drive using a 32-bit fixed-point DSP is built and tested. The inverter switching frequency is set at 10 kHz, and the sampling frequency is 15 kHz. An optical encoder is mounted on the shaft to compare the estimated position and the measured one. The drive parameters are the same as in Table 2.

A 500 Hz voltage is injected into the tested motor, and is superimposed with an SVV. The SVV commutates from 0° to 360° with 45° intervals and achieves a steady state within 6.5 s. The total current responses are shown in Fig. 14. Then a second-order BPF is adopted to extract 500 Hz currents (Fig. 15). The performance of this BPF is shown in Fig. 16. As is shown in Fig. 15, profiles of current responses are position dependent, and this is attributed to the injection of the SVV (i.e., the HF current is modulated by magnetic saturation). Due to the presence of a negative-sequence component, the amplitude of $i_{\alpha h}$ is not equal to that of $i_{\beta h}$.

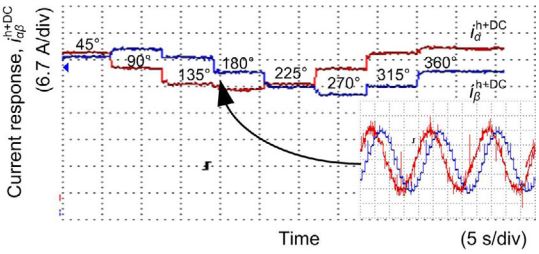

Fig. 14 Total current responses in the α-β frame

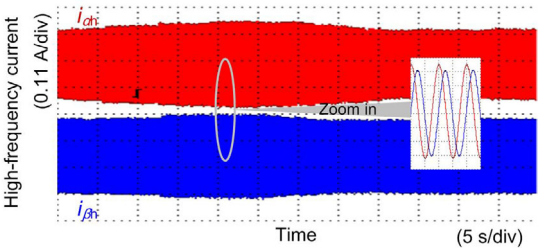

Fig. 15 Extracted 500 Hz current responses in the α-β frame

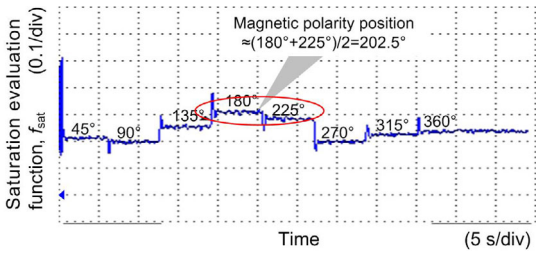

Fig. 16 Experimental process for identification of magnetic polarity

To saturate the iron core, 45% of the rated current is applied to the windings, and this will trigger rotation in the rotor. However, in heavy-duty applications, such as in starting HEVs, where the SPMSM

usually works as an auxiliary power unit (APU), the magnitude of the resisting torque is high and even a large current in the windings will not lead to shaft rotations.

Fig. 16 depicts the experimental results (filtered by LPF) for extraction of f_{sat}. During this procedure, values of f_{sat} are sampled at the end of each commutation of SVV. They are then stored in an array for post-processing in the DSP. In post-processing, the optimal and suboptimal angles are worked out by comparison, as illustrated in Fig. 6. As can be seen from Fig. 16, the experimental results are consistent with the simulation results; the median 202.5° is taken as the magnetic polarity, which approximates to the actual position 184.5°. The 500 Hz current is extracted with the methods shown in Eqs. (32) and (33). Hence, we obtain the negative-sequence component in HF currents. Fig. 17 shows the negative-sequence component, which includes a second-order harmonic (1 kHz) and a DC component. Passing the DC component through an inertial filter, we obtain the position error signal (Fig. 18).

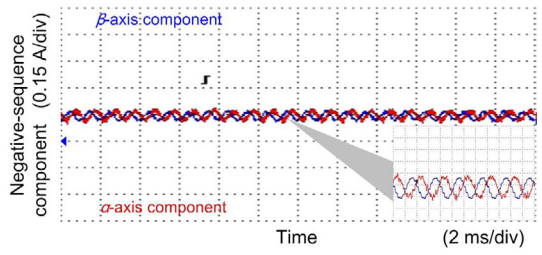

Fig. 17 Extracted negative-sequence components (References to color refer to the online version of this figure)

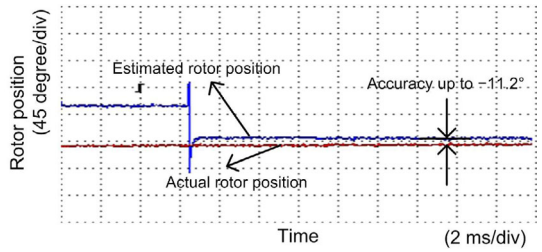

Fig. 18 Experimental results for the position observer

Next, the position observer is performed with an SVV located at 202.5°, which increases magnetism in the tested motor. This stage is similar to that of simulation, and the final estimation accuracy is −11.2°. Reasons for this error include ignorance of stator resistance, dead time of IGBTs, and sampling errors of ADCs. Fig. 19 shows the distribution of the estimation error versus the rotor position; the maximum error is 12.3° and the average error is 10.9° (absolute value). Comparison with conventional estimation methods for SPMSMs shows that the proposed strategy has a high precision.

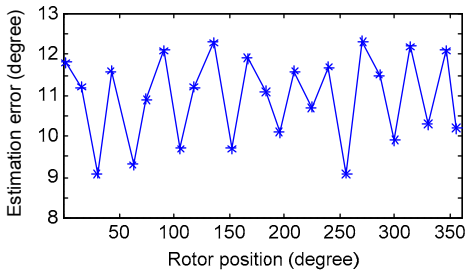

Fig. 19 Distribution of the estimation error versus rotor position

6 Conclusions

In this paper, we proposed an initial rotor position estimation for SPMSMs based on the nonlinear model with the hybrid injection of SVV and HF voltages. The injected SVV is used to alter machine saturation levels, and this saturation level is reflected in the HF current. Unlike conventional approaches for IPMSMs, the proposed method is based on the concept of saturating motors before estimating rotor position. Accordingly, a special demodulation algorithm is introduced, which uses only two second-order BPFs and three inertia filters. Based on the above demodulation, the saturation evaluation function and rotor position information are extracted. Thus, the position can be observed by a regular PI controller. The position estimation error of the proposed method is less than 13° (electrical), according to the simulation and experimental results. The proposed method can be a substitute for the Hall effect sensor for acquiring an accurate initial rotor position for starting HEVs.

References

Bolognani, S., Calligaro, S., Petrella, R., 2011. Design issues and estimation errors analysis of back-EMF based position and speed observer for SPM synchronous motors. Symp. on Sensorless Control for Electrical Drives, p.138-145.
http://dx.doi.org/10.1109/SLED.2011.6051558

El-Serafi, A.M., Wu, J., 1993. Determination of the parameters representing the cross-magnetizing effect in saturated synchronous machines. *IEEE Trans. Energy Conv.*, **8**(3):333-342. http://dx.doi.org/10.1109/60.257042

Fu, W.N., Ho, S.L., Zhang, Z., 2009. Design of position detection strategy of sensorless permanent magnet motors at standstill using transient finite-element analysis. *IEEE Trans. Magn.*, **45**(10):4668-4671. http://dx.doi.org/10.1109/TMAG.2009.2022406

Gao, W., Meliopoulos, A.P.S., Solodovnik, E.V., *et al.*, 2005. A nonlinear model for studying synchronous machine dynamic behavior in phase coordinates. IEEE Int. Conf. on Industrial Technology, p.1092-1097. http://dx.doi.org/10.1109/ICIT.2005.1600798

Harke, M.C., de Donato, G., Capponi, F.G., *et al.*, 2008. Implementation issues and performance evaluation of sinusoidal, surface-mounted PM machine drives with Hall-effect position sensors and a vector-tracking observer. *IEEE Trans. Ind. Appl.*, **44**(1):161-173. http://dx.doi.org/10.1109/TIA.2007.912729

Li, Y., Zhu, Z.Q., Howe, D., *et al.*, 2007. Modeling of cross-coupling magnetic saturation in signal-injection-based sensorless control of permanent-magnet brushless AC motors. *IEEE Trans. Magn.*, **43**(6):2552-2554. http://dx.doi.org/10.1109/TMAG.2007.892319

Liang, X.D., El-Serafi, A.M., Faried, S.O., 2010. Application of the finite-element method for the determination of the parameters representing the cross-magnetizing in saturated synchronous machines. *IEEE Trans. Energy Conv.*, **25**(1):70-79. http://dx.doi.org/10.1109/TEC.2009.2032535

Nakashima, S., Inagaki, Y., Miki, I., 2000. Sensorless initial rotor position estimation of surface permanent-magnet synchronous motor. *IEEE Trans. Ind. Appl.*, **36**(6):1598-1603. http://dx.doi.org/10.1109/28.887211

Seilmeier, M., Piepenbreier, B., 2011. Modeling of PMSM with multiple saliencies using a stator-oriented magnetic circuit approach. IEEE Electric Machines & Drives Conf., p.131-136. http://dx.doi.org/10.1109/IEMDC.2011.5994796

Sigmund, D., Lohner, A., Böh, M., *et al.*, 2014. Simulation-based development of an energy-management-system for a drive train of a parallel hybrid electric vehicle. 16th Int. Power Electronics and Motion Control Conf. and Exposition, p.822-827. http://dx.doi.org/10.1109/EPEPEMC.2014.6980599

Wang, Y., Zhu, J.G., Guo, Y.G., 2010. A comprehensive analytical mathematic model for permanent-magnet synchronous machines incorporating structural and saturation saliencies. *IEEE Trans. Magn.*, **46**(12):4081-4091. http://dx.doi.org/10.1109/TMAG.2010.2071392

Wang, Z., Niu, S.X., Ho, S.L., *et al.*, 2012. A position detection strategy for sensorless surface mounted permanent magnet motors at low speed using transient finite-element analysis. *IEEE Trans. Magn.*, **48**(2):1003-1006. http://dx.doi.org/10.1109/TMAG.2011.2173914

Yan, Y., Zhu, J.G., Guo, Y.G., 2008. Initial rotor position estimation and sensorless direct torque control of surface-mounted permanent magnet synchronous motors considering saturation saliency. *IET Electr. Power Appl.*, **2**(1):42-48. http://dx.doi.org/10.1049/iet-epa:20070083

Yang, S.C., 2015. Saliency-based position estimation of permanent-magnet synchronous machines using square-wave voltage injection with a single current sensor. *IEEE Trans. Ind. Appl.*, **51**(2):1561-1571. http://dx.doi.org/10.1109/TIA.2014.2358796